Pergamon

Geochimica et Cosmochimica Acta, Vol. 68, No. 20, pp. 4189-4200, 2004

0016-7037/04 $30.00 + .00

doi:10.1016/j.gca.2004.04.002

Nature of polymerization and properties of silicate melts and glasses at high pressure

SUNG KEUN LEE,*,† GEORGE D. CODY, YINGWEI FEI, and BJORN O. MYSEN

Geophysical Laboratory, Carnegie Institution of Washington, 5251 Broad Branch Rd., Washington, DC 20015 USA

(*Received October* 31, 2003; *accepted in revised form April* 2, 2004)

Abstract—The structures of sodium silicate and aluminosilicate glasses quenched from melts at high pressure (6–10 GPa) with varying degrees of polymerization (fractions of nonbridging oxygen) were explored using solid-state NMR [^{17}O and ^{27}Al triple-quantum magic-angle spinning (3QMAS) NMR]. The bond connectivity in melts among four and highly coordinated network polyhedra, such as $^{[4]}Al$, $^{[5,6]}Al$, $^{[4]}Si$, and $^{[5,6]}Si$, at high pressure is shown to be significantly different from that at ambient pressure. In particular, in the silicate and aluminosilicate melts, the proportion of nonbridging oxygen (NBO) generally decreases with increasing pressure, leading to the formation of new oxygen clusters that include 5- and 6-coordinated Si and Al in addition to 4-coordinated Al and Si, such as $^{[4]}Si$-O-$^{[5,6]}Si$, $^{[4]}Si$-O-$^{[5,6]}Al$ and Na-O-$^{[5,6]}Si$. While the fractions of $^{[5,6]}Al$ increase with pressure, the magnitude of this increase diminishes with increasing degrees of ambient-pressure polymerization under isobaric conditions. Incorporating the above structural information into models of melt properties reproduces the anomalous pressure-dependence of O^{2-} diffusivity and viscosity often observed in silicate melts. *Copyright © 2004 Elsevier Ltd*

1. INTRODUCTION

Silicate and aluminosilicate melts are dominant phases in the earth's crust and mantle and are key transport agents in the chemical evolution of the earth (Kushiro, 1976; Mysen, 1988). The properties of silicate melts at high pressure can provide important constraints on global geochemical processes, including mantle dynamics. The structure of silicate liquids at high pressure is centrally important for an understanding of the thermodynamic and transport properties of melts in the Earth's interior. Theoretical studies using molecular dynamics simulations (e.g., Angell et al., 1982) and experimental studies with conventional diffraction and spectroscopic methods have been applied to better understand the relationship between melt structures and properties at high pressure (see the review by Wolf and McMillan, 1995).

Previous high-pressure studies of the structure of silicate melts and glasses suggest that with increasing pressure, Si-O distances increase and bond angles (e.g., Si-O-Si) decrease in pure SiO_2 glasses (Hemley et al., 1986). The distortion of network polyhedra associated with Si-O bond length distribution has also been positively correlated with pressure (Devine and Arndt, 1987). The fraction of highly coordinated Si (e.g., 5 or 6 coordinated Si, $^{[5,6]}Si$) or Al in partially depolymerized melts (e.g., $Na_2Si_4O_9$ and $Na_3AlSi_7O_{17}$) gradually increases with pressure, a phenomenon that has been related to the anomalous transport properties of aluminosilicate melts, wherein the diffusivity first increases, then decreases with increasing pressure (Waff, 1975; Xue et al., 1989; Poe et al., 1997; Diefenbacher et al., 1998; Poe et al., 2001). This behavior depends on the composition (Si/Al ratio, nonbridging oxygen fraction, etc.) of the silicate melts (e.g., Scarfe et al., 1986). For example, the O^{2-} diffusivity of diopside ($CaMgSi_2O_6$) melts at high pressure shows a trend opposite to that of aluminosilicate melts (Kushiro, 1976; Shimizu and Kushiro, 1984). These early studies and subsequent experiments confirmed that the degree of polymerization of silicate liquids [e.g., the fraction of nonbridging oxygen (NBO) or NBO/T, T is four-coordinated framework cations] strongly affects their transport and thermodynamic properties as well as their pressure dependence (Kushiro, 1976; Dunn, 1983; Brearley et al., 1986; Tinker and Lesher, 2001; Behrens and Schulze, 2003; Tinker et al., 2003).

The polymerization of silicates at high pressure can also govern the distribution (or partitioning) of elements in the mantle (Mysen, 1988; Kushiro and Mysen, 2002). For example, structure of silicate melts (NBO/T) appears to determine the partitioning of Mg and Fe^{2+} between olivine and magmatic melts (Kushiro and Mysen, 2002). Therefore, if NBO/T of a melt varies with pressure, the Fe^{2+}-Mg equilibria between melt and olivine is also pressure-dependent.

Notwithstanding the importance of the nature of polymerization of silicate melts at high pressure, the effect of pressure on the structures and the extent of polymerization are largely unknown. The degree of polymerization (NBO/T) has often been deduced indirectly from the melt composition or pressure-dependent melt properties due to a lack of suitable experimental probes. Recent advances in solid state NMR, particularly ^{17}O 3Q (triple quantum) MAS NMR (Frydman and Harwood, 1995), make it possible to probe in some detail the atomic configuration around nonbridging oxygen and bridging oxygens (BO), to ascertain their populations, and to provide a direct measure of connectivity among framework units (e.g., Lee and Stebbins, 2002). We recently reported the first ^{17}O two-dimensional NMR spectra for binary silicate glasses quenched from melts at high pressure (10 GPa) in the multi-anvil apparatus, revealing previously unknown details of glass and melt structure at high pressure, including new oxygen sites such as $^{[4]}Si$-O-$^{[5,6]}Si$ (Lee et al., 2003). In addition to ^{17}O NMR, ^{27}Al MAS NMR has been useful for revealing the effect of pressure on Al coordination (Yarger et al., 1995). ^{27}Al

* Author to whom correspondence should be addressed (sungklee@snu.ac.kr).
† *Present address:* School of Earth and Environ. Sciences, Seoul National University, Seoul 151-742, Korea.

3QMAS NMR has improved prospects for Al coordination studies, even at relatively low static magnetic fields (e.g., 9.4 and 7.1 T; Lee and Stebbins, 2000b).

Here, we extend the previous study of silicate glasses and melt structure at high pressures (Lee et al., 2003) to aluminosilicate glasses and melts with varying pressure conditions and degrees of polymerization. These studies allow direct exploration of the evolution of oxygen site configuration as a function of pressure and composition. The chemical composition of the silicate glasses and melts studied here corresponds to NBO/T values appropriate for basaltic (depolymerized) to rhyolitic melts (fully polymerized). We also report ^{27}Al 3QMAS NMR spectra for aluminosilicate melts to examine how the coordination environment of Al changes with pressure. Finally, we present a model that seems to explain the anomalous pressure dependence of the transport properties of silicate melts.

2. EXPERIMENTS

2.1. Starting Materials and High-Pressure Glass Synthesis

Sodium silicate and aluminosilicate glasses along the pseudobinary join Na_2O-3SiO_2 (NS3)-$NaAlSi_3O_8$ (NAS6), including these end members and $(Na_2O)_{0.75}(Al_2O_3)_{0.25}3SiO_2$(NAS150560) composition glasses were synthesized from Na_2CO_3, Al_2O_3, and 40% ^{17}O-enriched SiO_2. Approximately 0.2 wt % of Co oxides was added to enhance the spin-lattice relaxation. The oxide-carbonate mixtures were decarbonated and fused for an hour at ambient pressure at 1200 to 1500 °C and then quenched. Negligible weight loss was observed during synthesis after accounting for decarbonation. The glass starting materials were loaded in a multi-anvil apparatus at the Geophysical Laboratory with a 10/5 (for 10 GPa) and an 18/11 (for sample synthesis below 8GPa; octahedron edge length/truncated edge length of the anvils) assembly. For a detailed design of the apparatus, see Bertka and Fei (1997). Each sample was fused at approximately 1650 to 1900 °C for 15 to 20 min, depending on their melting temperatures, and then quenched to glass by turning off power to the heater at 6 to 10 GPa. Initial quenching rate is approximately 500 °C/s.

The diameter of the quenched sample from the 18/11 assembly is slightly larger than the inner diameter of the 2.5 mm rotor used for the NMR experiments. Consequently, the sample was broken into small pieces comparable to the diameter of the rotor. The width of the sample obtained from the 10/5 assembly is smaller than that of the rotor, and the samples from this assembly were used without grinding them into powder, to prohibit possible hydration or to minimize the structural changes that may be associated with crushing and grinding the sample.

2.2. NMR Spectroscopy

Nuclear magnetic resonance spectra were collected on a CMX Infinity 300 spectrometer (7.1 tesla) at a Larmor frequency of 40.7 MHz for ^{17}O and 78.2 MHz for ^{27}Al. Experiments were run using a double resonance magic angle spinning (MAS) probe with a 2.5mm rotor. Recycle delays for ^{17}O and ^{27}Al MAS NMR were 1 s, with radio frequency pulse lengths of ~0.15 μs, which corresponds to a 15° tip angle for the central transition (1/2 ↔ -1/2) in solids. The ^{17}O and ^{27}Al 3QMAS NMR spectra were collected using a shifted-echo pulse sequence with acquisition parameters similar to those previously described (Lee et al., 2003). A sample spinning speed of 19 kHz was used. The spectra were referenced to external tap water for ^{17}O and 0.1 mol/L $AlCl_3$ for ^{27}Al.

3. RESULTS AND DISCUSSION

3.1. Structure of Sodium Silicate Glasses (NS3) Quenched From Melts at High Pressure

Figure 1 presents the typical ^{17}O MAS and 3QMAS NMR spectra of sodium trisilicate glasses quenched from melts at 8 GPa (NS3_8GPa). As described previously (Lee et al., 2003), the narrow (around 20 ppm) and broad peaks observed in the ^{17}O MAS NMR spectra are assigned to nonbridging oxygen (NBO) and bridging oxygen (BO), respectively. The ^{17}O 3QMAS NMR spectrum, on the other hand, provides consid-

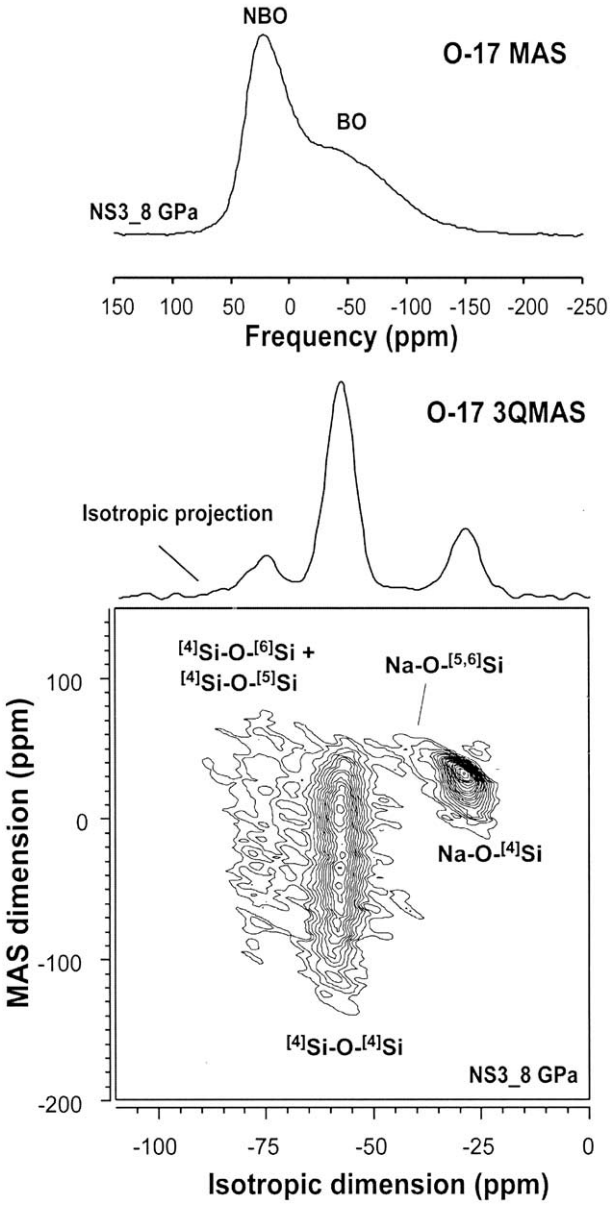

Fig. 1. ^{17}O MAS and 3QMAS NMR spectra of Na_2O-3SiO_2 glass (NS3) quenched from melts at 8 GPa (NS3_8GPa). The contour lines are drawn from 8 to 98% with 5% increments and additional 4 and 6% lines. For a spin-5/2 nuclei (^{27}Al and ^{17}O), the center of gravity in the isotropic dimension in 3QMAS NMR spectra (δ_{3qmas}) is given by $\delta_{3QMAS} = -17/31\delta_{iso}^{CS} + 10/31\delta_{iso}^{2Q}$ while the center of gravity of the same peak in the MAS dimension (δ_{MAS}) can be expressed as, $\delta_{MAS} = \delta_{iso}^{CS} + \delta_{iso}^{2Q}$. Here, δ_{iso}^{CS} and δ_{iso}^{2Q} are the isotropic chemical shift and the second-order quadrupolar shift, respectively (Baltisberger et al., 1996; Lee and Stebbins, 2000b). Note that the isotropic dimension of 2-dim. spectra is plotted in the opposite sense to that portrayed in the to 1-dim. MAS spectra.

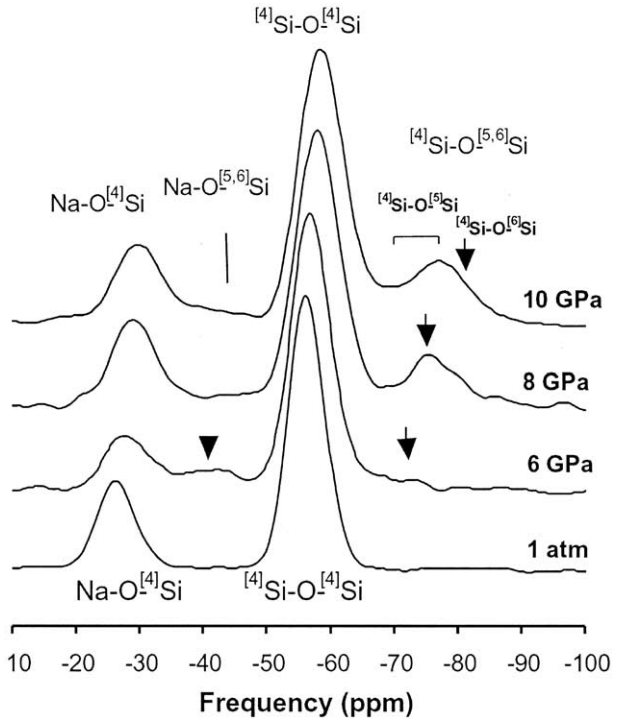

Fig. 2. Total isotropic projection of ^{17}O 3QMAS NMR spectra for Na_2O-3SiO_2 glasses quenched from melts at varying pressure as labeled (7.1 tesla). The chemical shift range for [5]Si-O-[4]Si in the 3QMAS (isotropic) dimension is from quantum chemical calculations (Lee et al., 2003). The arrow at about -82 ppm at 10 GPa indicates the predicted peak position for wadeite ($K_2Si_4O_9$; Xue et al., 1994).

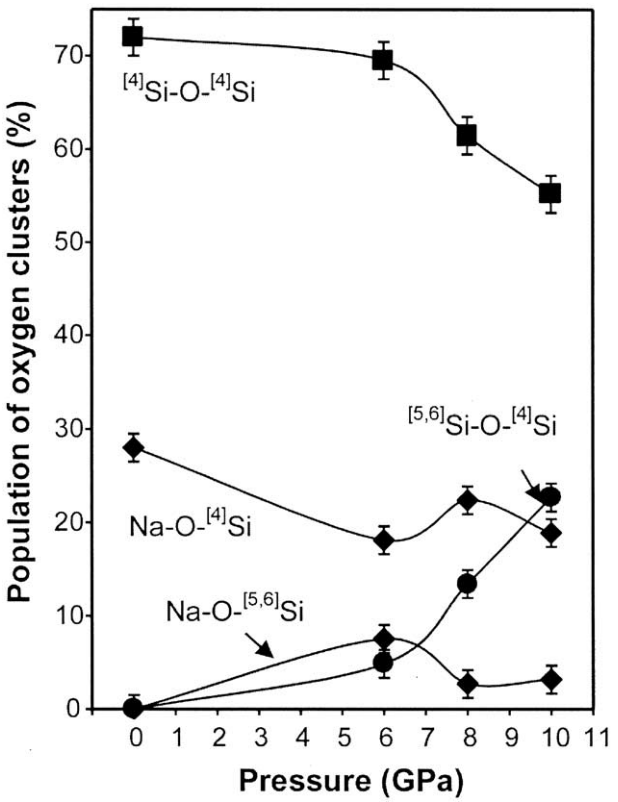

Fig. 3. Variation of oxygen cluster population with pressure in Na_2O-3SiO_2 glasses. Closed diamonds, squares, circles and diamonds refer to Na-O-[4]Si, [4]Si-O-[4]Si, [5,6]Si-O-[4]Si, and Na-O-[5,6]Si, respectively. Thick curves show trend line connecting experimental data.

erably improved resolution, revealing two NBO sites (Na-O-[5,6]Si and Na-O-[4]Si) and two BO sites ([4]Si -O-[5,6]Si and [4]Si-O-[4]Si). These data clearly demonstrate that the structure of melts at high pressures differs considerably from that at ambient pressure; NS3_amb has only one type of NBO (Na-O-[4]Si) and BO ([4]Si-O-[4]Si). Total isotropic projection spectra (the sum of the 2D NMR data in the isotropic dimension) also reveal the additional oxygen clusters at high pressure, and thus, we mainly present the isotropic projections of 2D 3QMAS spectra for the glasses studied here (see below). The isotropic projection usually yields a spectrum free from residual second-order quadrupolar broadening, and the projection on the MAS dimension provides a spectrum comparable with conventional 1 dim. MAS NMR. Structurally relevant NMR parameters can be obtained from the center of gravity of each peak in 3QMAS NMR spectra (see Figure caption 1; and also Baltisberger et al. (1996); Lee and Stebbins, (2000b)).

Figure 2 presents a total isotropic projection of NS3 quenched from melts at varying pressure from 1 atm to 10 GPa. It is clear that the fraction of [4]Si-O-[5,6]Si, indicated by increasing intensities between −70 to −80 ppm, increases with increasing pressure.

Na-O-[5,6]Si (inverse triangle, Fig. 2) appears to form preferentially over [4]Si-O-[5,6]Si at ~6 GPa as observed by noticeable spectral intensity increase at approximately -40 ppm in the isotropic dimension of the spectra. One plausible mechanism for pressure-induced structural changes, therefore, involves the annihilation of Na-O-[4]Si and formation of the other types of NBO, such as Na-O-[5,6]Si. A possible structural scheme consistent with this observation would have NBOs in Q_3 (3 BO and 1 NBO for 4-coordinated Si) and Q_2 (2BO and 2NBO for 4 coordinated Si) combining to form Na-O-[5]Si:

$$2\text{Na-O-}^{[4]}\text{Si}(Q_2) + \text{Na-O-}^{[4]}\text{Si}(Q_3) = 2\text{Na-O-}^{[5]}\text{Si}(P^5_3)\text{-O-}^{[4]}\text{Si}(Q_4) + \text{Na}^* \quad (1.1)$$

where Na* is a charge-balancing cation that does not contribute to formation of NBO, and where $P^5{}_3$ refers to 5-coordinated Si cluster with 2NBO and 3BO.

Above 6 GPa, it is likely that [4]Si-O-[5,6]Si forms at the expense of both Na-O-[4]Si, [4]Si-O-[4]Si (Xue et al., 1991), as well as Na-O-[5,6]Si:

$$\text{Na-O-}^{[4]}\text{Si} + \text{Na-O-}^{[5,6]}\text{Si} = \text{Na-O-}^{[4]}\text{Si-O-}^{[5,6]}\text{Si} + \text{Na}^*. \quad (1.2)$$

$$\text{Na-O-}^{[4]}\text{Si} + {}^{[4]}\text{Si-O-}^{[4]}\text{Si} = {}^{[4]}\text{Si-O-}^{[5,6]}\text{Si} + \text{Na}^*. \quad (1.3)$$

These mechanisms (Eqn. 1.1.–1.3) highlight the changes in role of Na from a charge-modifying cation to a charge-balancing cation, while the total degree of melt polymerization increases. Figure 3 illustrates the effect of pressure on the oxygen cluster population in sodium silicate glasses. The oxygen site populations were obtained by fitting the total isotropic projection with multiple Gaussian peaks. These intensities are normalized by considering the 3QMAS efficiency of each oxygen cluster (e.g.,

Lee and Stebbins, 2000b). It is observed that the fraction of $^{[4]}$Si-O-$^{[4]}$Si decreases slightly with pressure (by ~2 to 4% of the total fraction) up to 6 GPa and then significantly decreases, from 70 to 55% between 6 GPa and 10 GPa. This decrease suggests that Q_3 and Q_4 species (and thus the BO) participate further pressure-induced structural changes above 6 GPa as suggested in Eqn. 1.1 and Eqn. 1.2. The fraction of $^{[5,6]}$Si-O-$^{[4]}$Si also exhibits a positive correlation with pressure. NBOs (Na-O-$^{[4]}$Si and Na-O-$^{[5,6]}$Si) in sodium silicate glasses reveal intriguing pressure dependences near 6 GPa. The Na-O-$^{[4]}$Si fraction decreases by ~10%, reflecting formation of Na-O-$^{[5,6]}$Si at 6 GPa. Above 6 GPa, however, the Na-O-$^{[4]}$Si fraction increases up to 8 GPa while the fraction of Na-O-$^{[5,6]}$Si decreases. These changes are accompanied by the formation of $^{[5,6]}$Si-O-$^{[4]}$Si, as shown in Figure 2 and Eqn. 1.2. These structural responses to pressure suggest that initial structural changes of silicate melts with pressure primarily involve interactions among the NBOs rather than those between NBO and BO.

The peak width in the NMR spectra of each oxygen site increases with increasing pressure, consistent with increasing topological disorder, e.g., broadening of bond length and angle distribution (see below for further discussion). A systematic peak shift (e.g., $^{[4]}$Si-O-$^{[4]}$Si) is observed in the isotropic dimension (Fig. 2) and is primarily due to an increased isotropic chemical shift with pressure as opposed to 2nd order quadrupolar shift. Detailed analysis of variation of NMR parameters with pressure can be found in the recent report (Lee, 2004). Whereas it is difficult to distinguish the contribution of $^{[5]}$Si-O-$^{[4]}$Si from that of $^{[6]}$Si-O-$^{[4]}$Si because of peak overlap, the contribution from the $^{[6]}$Si-O-$^{[4]}$Si peak appears to increase with pressure, as shown in the isotropic projection for 6 GPa and 10 GPa glasses (Fig. 2, arrows).

3.2. Structure of $(Na_2O)_{0.75}(Al_2O_3)_{0.25}3SiO_2$ Glasses (NAS150560) Quenched From Melts at High Pressure

It is well known that the degree of polymerization in silicate melts increases when Al_2O_3 replaces Na_2O in peralkaline Na-silicate glasses at 1 atm (e.g., Mysen et al., 1982). Thus NAS150560 is more polymerized than NS3. Figure 4 presents the ^{27}Al 3QMAS NMR spectra for this sodium aluminosilicate glass as a function of pressure. The fraction of highly coordinated $^{[5,6]}$Al clearly increases with increasing pressure, consistent with previous reports from high-field ^{27}Al MAS NMR for sodium aluminosilicate glasses (Yarger et al., 1995).

Figure 5 presents the total isotropic projection of the ^{17}O 3QMAS NMR spectra of NAS150560. At 1 atm, a single type of NBO (Na-O-$^{[4]}$Si) and two types of BOs ($^{[4]}$Si-O-$^{[4]}$Si and $^{[4]}$Si-O-$^{[4]}$Al) are observed. With increasing pressure, both the Na-O-$^{[4]}$Si and $^{[4]}$Si-O-$^{[4]}$Al oxygen cluster populations decrease for NS150560. These trends suggest the following structural changes with pressure:

$$\text{Na-O-}^{[4]}\text{Si} + {}^{[4]}\text{Si-O-}^{[4]}\text{Al} = {}^{[4]}\text{Si-O-}^{[5,6]}\text{Al} + \text{Na}^{*}. \quad (2)$$

Note that there is a negligible fraction of $^{[4]}$Si-O-$^{[5,6]}$Si in NAS150560 at 8 GPa, unlike in the NS3. These results suggest that the decrease of Na-O-$^{[4]}$Si is mainly connected with the formation of highly coordinated Al. This conclusion is consistent with previous reports that Al is more likely than Si to be highly coordinated (e.g., Waff, 1975; Poe et al., 1997). In

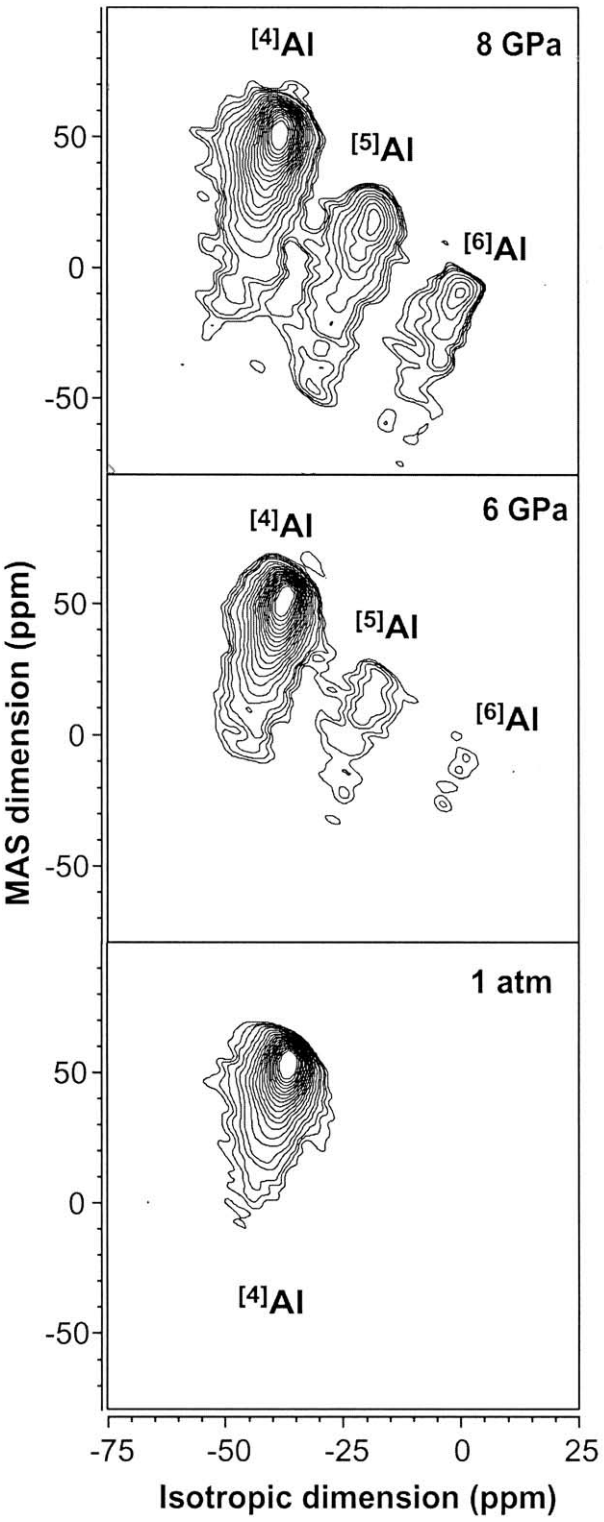

Fig. 4. ^{27}Al 3QMAS NMR spectra (7.1 tesla) for $(Na_2O)_{0.75}(Al_2O_3)_{0.25}$ $3SiO_2$ glasses (NAS150560) quenched from melts at varying pressure as labeled. The contour lines are drawn from 8 to 98% with 5% increments and an additional 4% line.

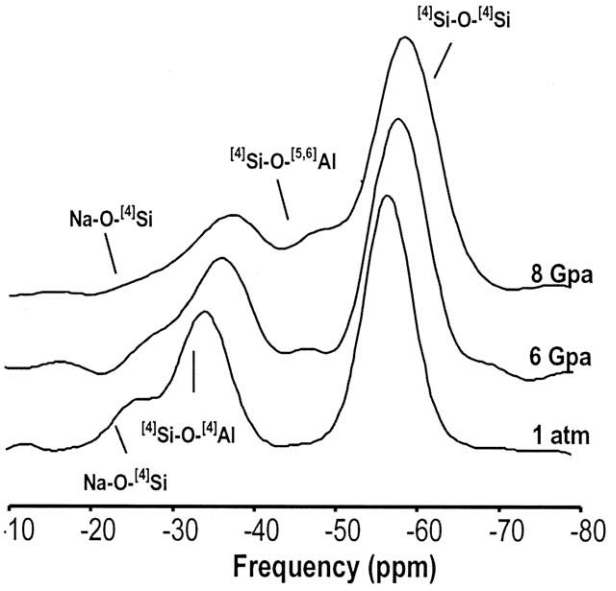

Fig. 5. Total isotropic projection of ^{17}O 3QMAS NMR spectra (7.1 tesla) for $(Na_2O)_{0.75}(Al_2O_3)_{0.25}3SiO_2$ glasses with varying pressure.

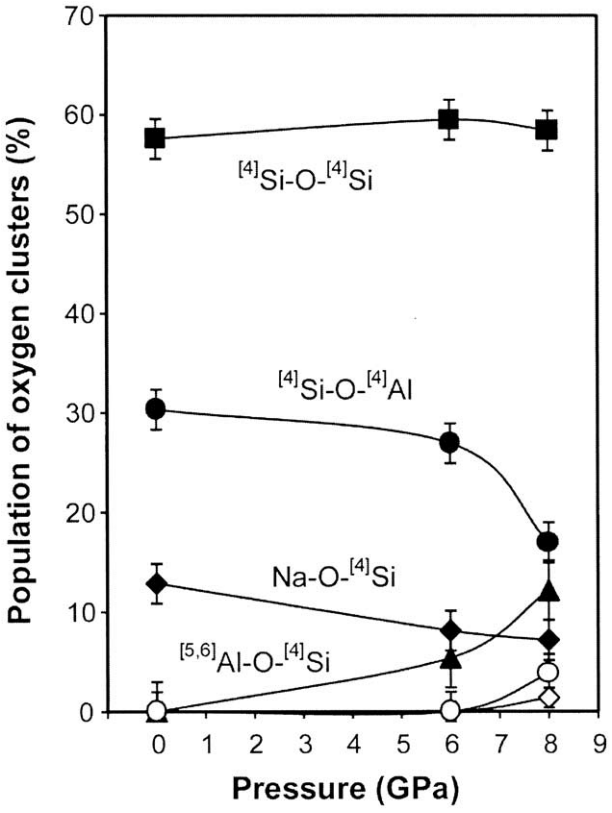

Fig. 6. Variation of oxygen cluster population with pressure in NAS150560 aluminosilicate glasses. Closed circles, diamonds, squares, and triangle refer to [4]Al-O-[4]Si, Na-O-[4]Si, [4]Si-O-[4]Si, and [5,6]Al-O-[4]Si, respectively. Open circles and diamond denote [5,6]Si-O-[4]Si and Na-O-[5,6]Si.

Figure 6 the oxygen cluster population for each cluster in NAS150560 with varying pressure is summarized. One-dimensional isotropic projections do not reveal low abundances of Na-O-[5]Si due to peak overlap with [4]Si-O-[4]Al. Small contribution in spectra intensity due to Na-O-[5]Si can be resolved in 2D spectra as discussed further below (Fig. 10).

3.3. Structure of $NaAlSi_3O_8$ Glasses (NAS6) Quenched From Melts at High Pressure

NAS6 glasses are fully or nearly fully polymerized at 1 atm, and thus provide a good model system to assess pressure-induced structural changes that do not involve NBO. Figure 7 presents ^{27}Al 3QMAS NMR spectra of NAS6, which shows evidence of some [5]Al at NAS6 glasses quenched from melts at 8GPa (NAS6_8GPa), whereas only [4]Al is present at NAS6_1atm. In Figure 8 the effect of pressure on Al coordination in NAS6 and NAS150560 is compared. It is observed that, in both cases, the fraction of [4]Al decreases with pressure, whereas [5]Al and [6]Al species increase. However, the total fractions of high coordinated Al ([5]Al + [6]Al) in NAS150560_8GPa is ~37%, which is much larger than that in NAS6_8GPa (~7 to 8% and negligible amount of [6]Al). This observation confirms that the formation of [5]Al in aluminosilicate melts is facilitated by the presence of NBO. Small fractions of [5]Al may suggest the presence of tricluster (oxygen coordinated by three framework units) or edge-shared oxygens.

Figure 9 shows the total isotropic projections of ^{17}O 3QMAS NMR spectra for $NaAlSi_3O_8$ (NAS6) glasses quenched from melts at 1 atm and at 8 GPa. At 1 atm, two types of bridging oxygen ([4]Si-O-[4]Al and [4]Si-O-[4]Si) are observed (Dirken et al., 1997; Xu et al., 1998; Lee and Stebbins, 2000a). At 8 GPa, these BO peaks shift toward higher frequency (more negative in the isotropic dimension). This shift may suggest that the Al-O and Si-O bond lengths increase, and thus intertetrahedral bond angles ([4]Si-O-[4]Al and [4]Si-O-[4]Si) are likely to be smaller (Lee et al., 2003) as suggested from crystalline aluminosilicates (Brown et al., 1969). Spectral intensity near -45 ppm in the isotropic projection for NAS6_8GPa may suggest the presence of [4]Si-O-[5,6]Ai (Fig. 9, arrow). The presence of tricluster or nonbridging oxygen is not obvious because of insufficient signal/noise in the two-dimensional NMR spectra of NAS6_8 GPa, as well as because of possible peak overlap with other BO peaks. It should be noted that [4]Si-O-[4]Si clusters in NAS6 are also subject to topological adjustment comparable to [4]Si-O-[4]Al (reducing the intertetrahedral angle) as suggested from similar peak shifts for both clusters in the isotropic dimension (Fig. 9). [4]Si-O-[4]Si clusters in NAS150560 (Fig. 5), on the other hand, appear to exhibit less topological variation than those in NAS6 with pressure, as suggested by relatively smaller peak shift and narrow peak width in isotropic dimension (Fig. 9). This implies that NAS6 is subject to more severe topological (bond angle and bond length) rearrangement with pressure than are depolymerized aluminosilicates (NAS150560) that form highly coordinated Al species.

3.4. The Degree of Polymerization of Silicate Melts at High Pressure

Figure 10 shows ^{17}O 3QMAS NMR spectra of the three silicate glasses quenched from melts at 8 GPa. These spectra illustrate the

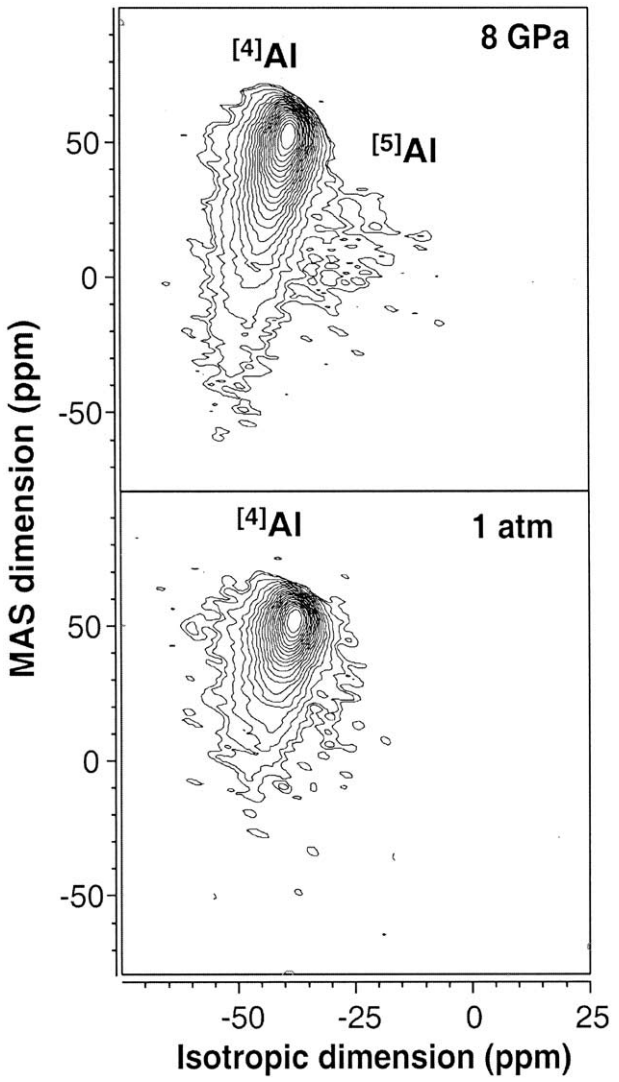

Fig. 7. ^{27}Al 3QMAS NMR spectra (7.1 tesla) for $NaAlSi_3O_8$ glasses quenched from melts at varying pressure as labeled. The contour lines are drawn from 8 to 98% with 5% increments and an additional 4% line.

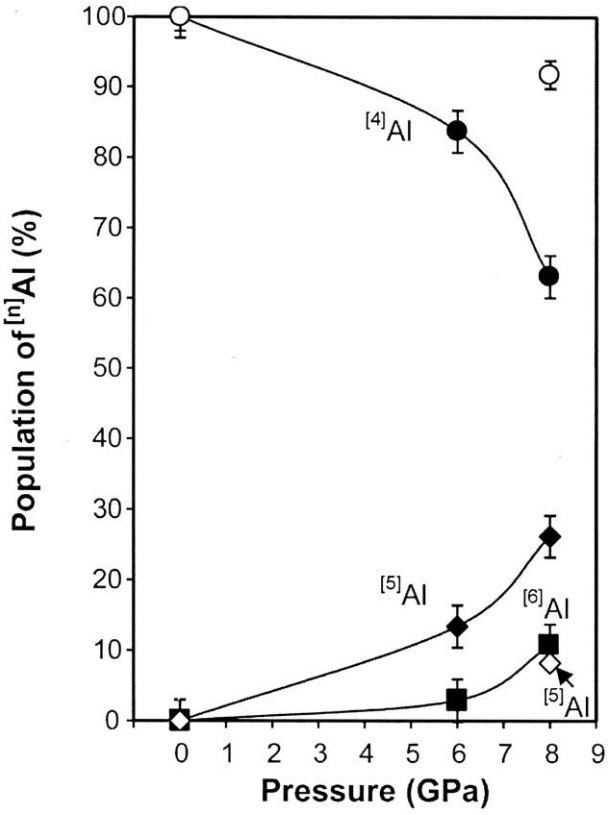

Fig. 8. Populations of Al sites with pressure. Circles, diamonds, and squares refer to fractions (%) of $^{[4]}$Al, $^{[5]}$Al, and $^{[6]}$Al, respectively. Open and closed symbols denote Al sites in $NaAlSi_3O_8$ glasses and NAS150560 glasses, respectively. We believe that the thick solid line shows the trend line for $^{[4]}$Al in NAS150560 glass.

connectivity among framework units in silicate melts with varying degrees of polymerization at high pressure. These spectra also provide detailed structural information on the effect of composition on NBO and BO. As for depolymerized, Al-free, sodium silicate glasses, the major structural changes with pressure involve the formation of $^{[5,6]}$Si, primarily at the expanse of NBO. As was shown previously (Lee et al., 2003), the oxygen clusters at high pressure are consistent with the chemical ordering among framework units, favoring oxygen-linking of dissimilar types of framework units, such as $^{[4]}$Si-O-$^{[5,6]}$Si.

Increased polymerization in melts and glasses at 1 atm occurs through Al for Na replacement (e.g., from NS3 to NAS150560). This leads to the formation of $^{[4]}$Si-O-$^{[4]}$Al. Note that neither $^{[4]}$Al-O-$^{[4]}$Al nor Na-O-$^{[4]}$Al species were observed. This provides another example of chemical ordering among framework units at 1 atm. At higher pressure, Al tends to be more highly coordinated than Si, which specifically forms $^{[4]}$Si-O-$^{[5,6]}$Al. The major mechanism of pressure-induced structural changes is again the reduction of NBO, increasing the total fraction of BO (Eqn. 2). In the case of fully polymerized melts (NAS6), no clear evidence is found of NBO or tricluster oxygen at 8 GPa, although the presence of a small fraction of $^{[5]}$Al implies that some of these species might be present. The connectivity of framework units in NAS6 quenched from melts at 8 GPa is similar to that at 1 atm; e.g., $^{[4]}$Si-O-$^{[4]}$Al and $^{[4]}$Si-O-$^{[4]}$Si are the predominant oxygen clusters. Those formed at high pressure, however, may have smaller average bond angle, as discussed above. Figure 11 presents the pressure dependence of the fraction of NBO (Na-O-$^{[4]}$Si + Na-O-$^{[5,6]}$Si) and BO (the sum of all the other oxygen clusters) in NS3 and NAS150560 (as shown in Figs. 3 and 6). The variation of $\partial X_{NBO}/\partial P$ appears to depend on both Si/Al and NBO fraction of silicate melts at 1 atm.

The three glass compositions studied here share common structural characteristics upon pressurization. The T-O bond length seems to increase, as evidenced by peak shifts in the isotropic projection of ^{17}O 3QMAS NMR spectra (Lee et al., 2003). In addition, the distribution of T-O or T-O-T may be wider with increasing pressure as inferred from the increase in peak width for BO and NBO in the NMR spectra with pressure (Figs. 2 and 5). The broadening of these internal variables obviously results in the increase in the topological disorder (Lee and Stebbins, 2003). On the other hand, chemical ordering

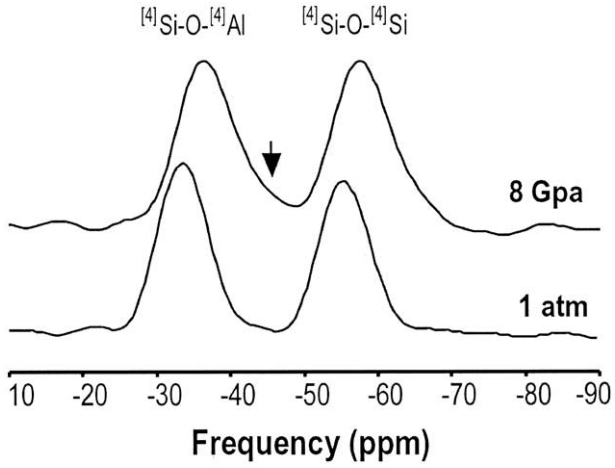

Fig. 9. Total isotropic projection of ^{17}O 3QMAS NMR spectra (7.1 tesla) for $NaAlSi_3O_8$ glasses quenched from melts at varying pressure as labeled.

in the framework distribution at ambient pressure favors dissimilar pairs, and ordering among NBOs precludes Na-O-[4]Al, even at high pressures (Fig. 10). Furthermore, there is chemical ordering among highly coordinated framework units at high pressure. This chemical ordering behavior is likely to decrease the configurational enthalpy and entropy of the silicate melts (see Lee and Stebbins (2002) for detailed discussion) and, therefore, lowers the activity coefficient of silica in high-pressure silicate melts in equilibrium with mantle mineral assemblages (Lee and Stebbins, 2003; Lee et al., 2003).

3.5. Modeling of Pressure Dependence of Transport Properties of Silicate Melt

One of the outstanding geochemical problems involves relating the structure of melts to macroscopic transport properties, which can provide improved prospects for understanding magmatic processes such as magma mixing and assimilations (Kushiro, 1983). As shown above, the detailed connectivity among framework units of silicate melts at high pressure can be directly estimated from two-dimensional ^{17}O 3QMAS NMR data. Such information can be used to develop a semiquantitative model to describe transport properties (e.g., effective diffusivity of O^{2-} and viscosity) of silicate melts that show anomalous pressure dependence as mentioned previously. The objective of modeling is to derive a phenomenological relationship between the nature of polymerization and transport properties of melts. No attempt is made to provide a quantitatively rigorous solution for complex melt properties.

The diffusion of O^{2-} in silicate melts may be described by considering two different processes, cooperative and noncooperative (primarily) bond breaking. In this modeling, it is assumed that O^{2-} diffusion involving NBOs is more cooperative (i.e., employing molecular-scale rearrangement) than the process with BO's. These constraints can be used to model the composition-dependent activation energy barrier for O^{2-} diffusion. In addition, we assume that the activation energy can be decomposed into primarily pressure-dependent terms and a

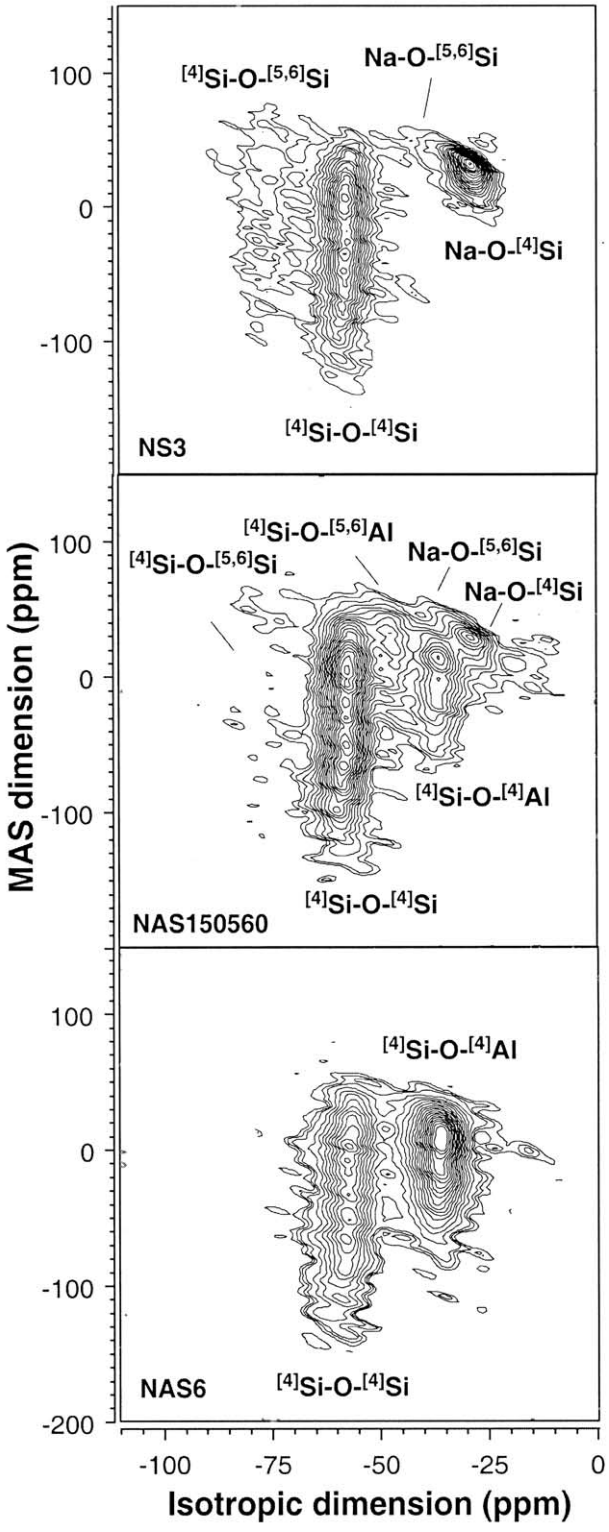

Fig. 10. ^{17}O 3QMAS NMR spectra for NS3 (top), NAS150560 (middle), and NAS6 glasses (bottom) quenched from melts at 8 GPa. The contour lines are drawn from 8 to 98% with 5% increments and additional lines at 4 and 6%.

temperature-dependent term. Given the assumptions and another conditions as described below, the total activation energy barrier for transport of O^{2-} may be written as follows:

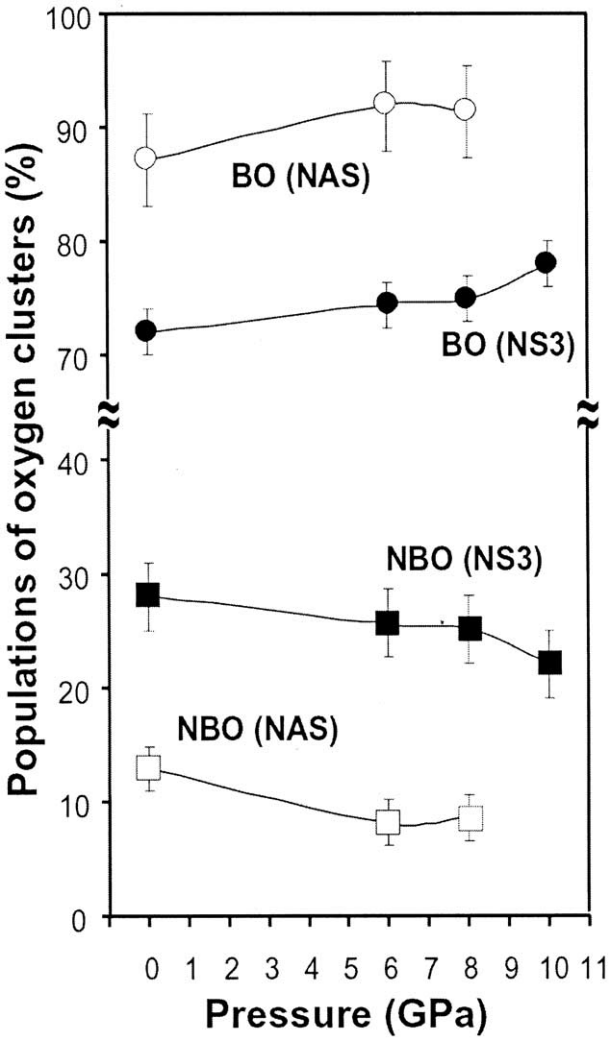

Fig. 11. Variation of total NBO and BO fractions with pressure in sodium silicate glasses (NS3, closed symbols) and aluminosilicate glasses (NAS refers to NAS150560, open symbols).

$$E(P, T, X) = [X_{NBO}(P)E_{NBO}(P) + X_{BO}(P)E_{BO}(P)]\frac{E_0}{T_g(X)}\left(\frac{T}{T_g(X)}\right)^{\frac{-F(X)}{1-F(X)}}, \quad (3)$$

where the terms inside the square bracket mainly describe the pressure dependence of activation energy barrier. The X_{NBO} and X_{BO} are the pressure-dependent fractions of NBO and BO, respectively (as shown in the ^{17}O 3QMAS NMR spectra of silicate and aluminosilicate glasses quenched from melts at high pressure in Figs. 2, 4, and 11). E_{NBO} is defined to be the activation energy barrier that is responsible for the diffusion of oxygen when the system consists of mostly NBO (note that this is a hypothetical limit), and E_{BO} is the activation energy that is mostly responsible for the diffusion of oxygen when the system is fully polymerized. This definition assumes that the variation of activation with composition (X_{NBO}) is linear (without considering the terms outside of the bracket), which seems a reasonable first approximation as was evidenced from the viscosity vs. X_{NBO} plot (Fig. 12). The former

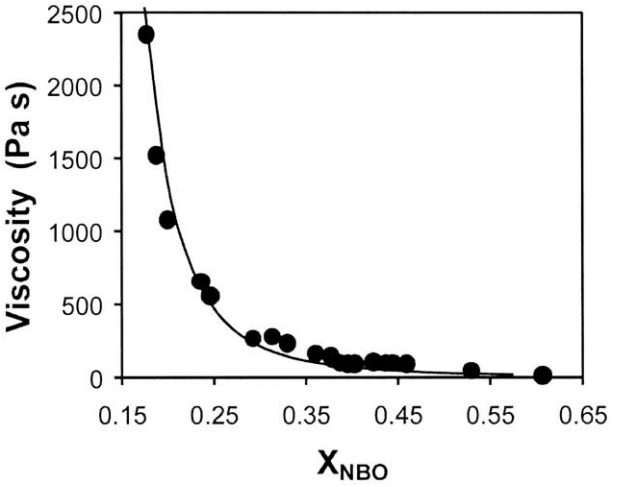

Fig. 12. The variation of viscosity with NBO fraction in sodium silicate melts at 1473 K. Circle refers to experimental data (Mazurin, 1983) and thick line shows a trendline (Eqn. 6).

is likely to be smaller than the latter, because E_{BO} is mainly related to bond breaking, whereas E_{NBO} may mainly stem from the molecular-scale rearrangement. The diffusion of NBO and BO also involves interconversion between them, which would have to be considered in a more rigorous model. Briefly, this could be an important contribution to understanding the diffusion process. One of the reviewers of this manuscript carefully indicated the fact that the conversion from NBO to BO may show negative activation volume, similar to the case in associatively activated ligand-exchange reactions in solutions. The term E_0 is constant. $T_g(X)$ is a composition-dependent glass transition temperature, and F(X) is fragility, which varies from 1 (fragile, a deviation from Arrhenian behavior over a specified temperature range is large) to 0 (strong, classical Arrhenian behavior) (Angell, 1995; Rao et al., 2001). The terms outside the square brackets can thus account for the temperature dependence of the activation energy barrier (Rao et al., 2001) where the temperature dependence of the activation energy barrier increases with increasing fragility. T_g varies little with pressure (Rosenhauer et al., 1979), and it is assumed to be independent of pressure in the present case. It is reasonable to assume that the fragility should vary with pressure and potentially be important to transport properties near the glass transition. On the other hand, for much higher temperatures than T_g, the diffusivity exhibits Arrhenian behavior (Shimizu and Kushiro, 1984) as does melt viscosity (e.g., Richet, 1984). We therefore assumed the fragility to be invariant with pressure in the present modeling, leaving the terms inside the square brackets as the only pressure-dependent terms in Eqn. 3.

Accepting these simplifying assumptions, the pressure dependence of the effective oxygen diffusion [$D(O^{2-})$] is given as:

$$\left(\frac{\partial D(O^{2-})}{\partial P}\right)_T \propto -\left[(E_{NBO} - E_{BO})\left(\frac{\partial X_{NBO}}{\partial P}\right)_T + X_{NBO}\left(\frac{\partial E_{NBO}}{\partial P}\right)_T + X_{BO}\left(\frac{\partial E_{BO}}{\partial P}\right)_T\right]. \quad (4)$$

The effect of composition to $(\partial D/\partial P)_T$ comes from the terms inside the bracket in Eqn. 3. Similarly, the viscosity of the melt may be also proportional to the quantity inside the square brackets in Eqn. 4, assuming Stokes-Einstein relations [$\eta = kT/(6\pi\lambda D(O^{2-}))$, where k is the Boltzman constant and λ is atomic jump distances]. The pressure dependence of viscosity can thus be expressed as follows (from $\partial D/\partial P = -\partial\eta/\partial P$):

$$\left(\frac{\partial \eta}{\partial P}\right)_T \propto \left[(E_{NBO} - E_{BO})\left(\frac{\partial X_{NBO}}{\partial P}\right)_T + X_{NBO}\left(\frac{\partial E_{NBO}}{\partial P}\right)_T + X_{BO}\left(\frac{\partial E_{BO}}{\partial P}\right)_T \right]. \quad (5)$$

Note that there can be decoupling of the viscosity from diffusivity of O^{2-} with varying composition, temperature, and pressure where Stokes-Einstein relationship is no longer valid. Whereas the sign for each term in Eqn. 4 and Eqn. 5 for silicate melts can depend on the characteristics of each system, there are several common features. First, the sign of E_{NBO}-E_{BO} is negative as discussed above. Below a threshold pressure (P_c) where highly coordinated framework units form, or in pressure ranges where only small fractions of highly coordinated framework units are present, $\partial X_{NBO}/\partial P \approx 0$. P_c is typically ~4 to 8 GPa (Figs. 3 and 6; Xue et al., 1991; Yarger et al., 1995). While it is probable that formation of small amounts of highly coordinated framework units occurs at the lower pressure, the small amount of these would not affect the properties, and thus, the results of the modeling given here. The signs of the pressure dependence of diffusivity and viscosity are, thus, mainly determined by the relative magnitudes of the last two terms of Eqn. 4 and Eqn. 5, respectively. $\partial E_{NBO}/\partial P$ is likely greater than 0 because molecular-scale readjustment may be prohibited by a possible decrease in free volume with pressure. $\partial E_{BO}/\partial P$ is largely negative due to increased T-O bond length with pressure: it would seem reasonable that the activation energy barrier of BO diffusion is likely to be inversely proportional to Si-O bond length as a first approximation. The Si-O bond length tends to increase with pressure as previously mentioned, resulting in a decrease in activation energy barrier, i.e., $\partial E_{BO}/\partial P < 0$. Therefore, in this modeling, it is assumed that the E_{NBO} has positive activation volume, while E_{BO} has negative activation volume (see Figure caption 13 for more information). These are consistent with the observation for negative activation volume for highly polymerized melts and positive activation volume for the melts with high NBO concentrations (e.g., Shimizu and Kushiro, 1984). Second, upon formation of highly coordinated framework units above P_c, $\partial X_{NBO}/\partial P < 0$. Therefore, the 1st and 2nd terms contribute positively to diffusivity, whereas the 3rd term contributes negatively.

The viscosity decreases with increasing concentration (or mole fraction) of network modifying cations (X_N) at ambient pressure (Mazurin, 1983). In binary silicate melts, X_N has 1:1 correspondence with fractions of NBO [X_{NBO} = NBO/(BO+NBO) = $2X_N/(2-X_N)$] so that X_{NBO} increases with X_N. The decreasing viscosity with X_{NBO} in sodium silicate melts is illustrated in Figure 12 as an example. Here, the viscosity may be expressed as given below (solid line in Fig. 12), similar to a recent study on multicomponent melts (Giordano and Dingwell, 2003):

$$\eta \propto \exp[A/(B + X_{NBO})], \quad (6)$$

where A and B are constant. The pressure dependence, therefore, can be deduced:

$$\left(\frac{\partial \eta}{\partial P}\right)_T \propto -\left(\frac{\partial X_{NBO}}{\partial P}\right)_T. \quad (7)$$

As shown above, X_{NBO} decreases gradually with increasing pressure (Fig. 11). Therefore, the relationship of Eqn. 7 demonstrates that above P_c, where the NBO concentration begins to decrease noticeably, the viscosity of silicate melts increases (and $D(O^{2-})$ decreases) with increasing pressure, if we ignore the pressure dependence of other contributions. Setting $\partial E_{NBO}/\partial P = \partial E_{BO}/\partial P = 0$ in Eqn. 5 leads to Eqn. 7, suggesting that Eqn. 5 can be applied to more general cases. Below, we illustrate the variation of $D(O^{2-})$ with pressure, temperature and composition. The viscosity of melts can easily be obtained from the Stokes-Einstein relations. Here, we use the fraction of NBO (X_{NBO} = NBO/(BO+NBO)) as a measure of the degree of polymerization. While NBO/T is a useful term to describe the degree of polymerization in covalent oxide melts and glasses, the fraction of NBO can be effective, particularly at high pressure (and even at ambient pressure) where its pressure dependence can be independently obtained via ^{17}O NMR, and the coordination environments of the frameworks cations can be complicated as shown in Figures 7 and 10. Before proceeding in this direction, however, it is important to recall that the transport properties of silicate melts are complex functions of both long- and short-range interactions. Care should be taken for direct application of Eqn. 3 to real experimental data because of the several aforementioned assumptions, and the fact that it does not capture the complexity (composition, types of modifying cations, Si/Al, speciation, etc.) of the system. Further modeling considering interconversion between NBO and BO, and adding even more terms (pressure, temperature, and composition) for the determination of activation energy, can be formulated. The simple relationship given here avoids such complexity and, therefore, addresses the pressure dependence phenomenologically. The above conceptual approach does account for the effects of polymerization in silicate melts with microscopic observations, such as the fraction of nonbridging oxygen and its pressure dependence as illustrated below.

In Figure 13 the effect of pressure on $D(O^{2-})$ is presented. It is seen that the anomalous pressure dependence may be explained by the relative pressure dependences of the activation energy barriers and the reduction of nonbridging oxygens (see figure caption for relevant model parameters for the calculations). In Figure 13A the hypothetical variation in the fractions of NBO with pressure is shown, which is used for the modeling of melt properties. In the case of melts with $X_{NBO} = 0.3$, the sign of $(\partial D/\partial P)_T$ is positive before the reduction of the NBO fraction and becomes negative with further increase of pressure (Fig. 13 B). This result is consistent with experimental diffusivity-vs.-pressure trends for NAS6 and other partially depolymerized aluminosilicate glasses (Poe et al., 1997). With further depolymerization of melts ($X_{NBO} = 0.5$, and 0.65), the value of $(\partial D/\partial P)_T$ becomes progressively more negative, consistent with experimental results where the sign $(\partial D/\partial P)_T$ varies from positive to negative with decreasing polymerization (Shimizu

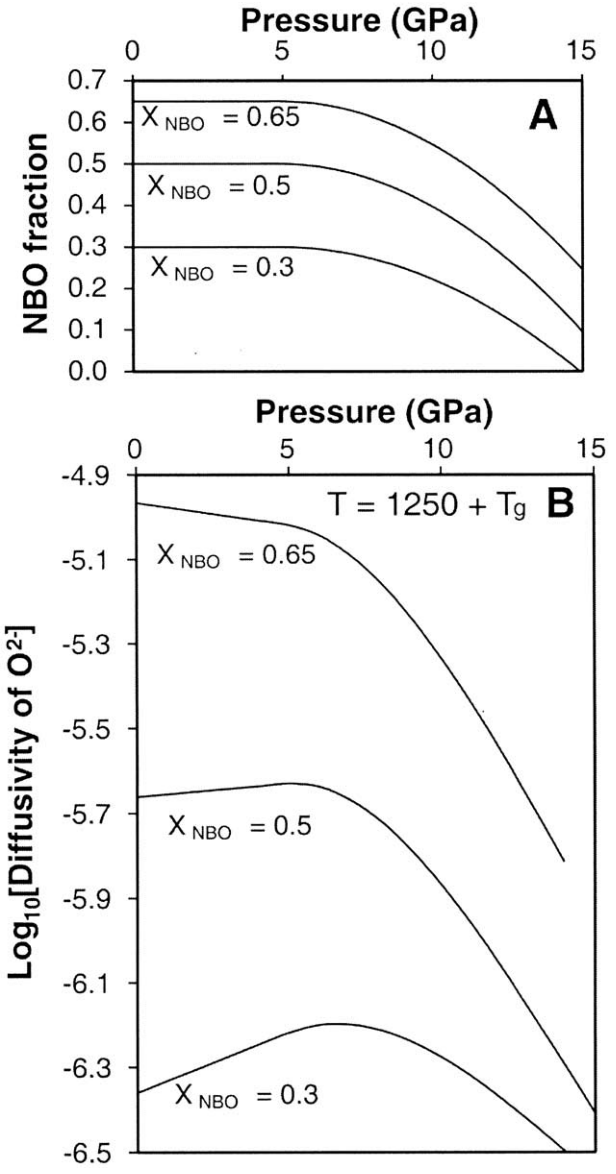

Fig. 13. A) Hypothetical variation of NBO fraction with pressure. B) Effect of pressure on O^{2-} diffusivity at constant temperature (T_g+1250 K), where T_g is the glass transition temperature that varies with fractions of NBO. Modeling conditions for T_g at X_{NBO} = 0.65, 0.5, 0.3 are set to 850, 750, and 675 K, respectively, and F(X_{NBO})s are 0.22, 0.3, and 0.36, respectively. The plots are also based on the relations for pressure dependent E_{NBO} (kJ/mol) [= 150 + 2 P (GPa)] and E_{BO} (kJ/mol) [= 300 - 2.5 P (GPa)]. Constant terms in E_{NBO} and E_{BO} can be comparable to typical activation energy for O^{2-} diffusion in silicate melts, and the pressure dependence can be comparable to experimental pressure dependent part of O^{2-} diffusion (activation volume) in silicate melts (e.g., Tinker and Lesher, 2001). Note that these modeling parameters are only for semiquantitative analysis for the *trend* of O^{2-} diffusivity.

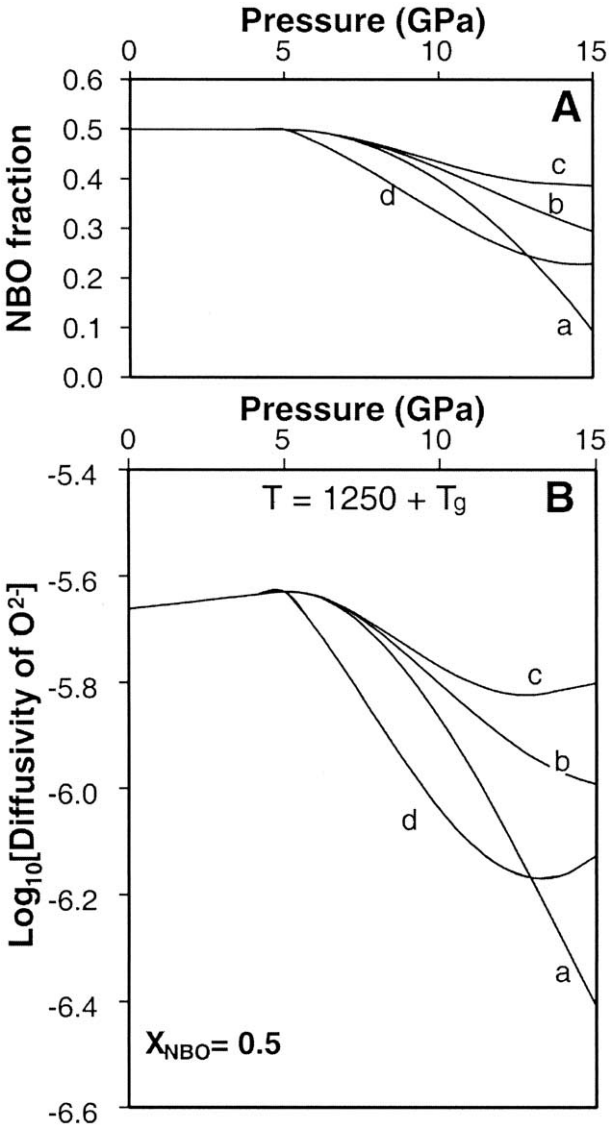

Fig. 14. Effect of pressure dependence of NBO fraction on O^{2-} diffusivity. A) variation of NBO fraction with pressure, B) corresponding O^{2-} diffusivity vs. pressure. Curve a, b, c, and d illustrate *hypothetical* pressure dependence of NBO fraction for modeling (A) and the corresponding variation of O^{2-} diffusivity (B). The identical modeling conditions to Figure 13 were used.

and Kushiro, 1984). Therefore the changes in the sign of $(\partial D/\partial P)_T$ or $(\partial \eta/\partial P)_T$ are heavily dependent on the pressure dependence of NBO, as well as the degree of polymerization (concentration of NBO).

Figure 14 illustrates the effect on $D(O^{2-})$ of varying $(\partial X_{NBO}/\partial P)_T$. It is seen that the pressure dependence of $D(O^{2-})$ is sensitive to the pressure dependence of X_{NBO}. For example, a monotonic decrease of X_{NBO} leads to a decrease in $D(O^{2-})$ (Fig. 14 A, curves a and b), the precise behavior depending on $(\partial X_{NBO}/\partial P)_T$ (Fig. 14 B). Furthermore, the sign of $(\partial^2 X_{NBO}/\partial^2 P)_T$ can change the sign of $(\partial D/\partial P)_T$, e.g., $D(O^{2-})$ increases with pressure if the sign of $(\partial^2 X_{NBO}/\partial^2 P)_T$ is positive (Fig. 14A, curves c and d). This may account for the pressure dependence of $D(O^{2-})$ in diopside ($CaMgSi_2O_6$) melts (X_{NBO} = 0.66 at 1 atm) up to 15 GPa. In this case, diffusivity decreases with increasing pressure below ~10 GPa, but increases above 10 GPa (Reid et al., 2001). As shown in Figure 11, the actual pressure dependence of the NBO fraction can be more fluctuating than the model behavior given in Figures 13 and 14. This implies more dramatic changes in melt

properties with pressure, which may agree with experimental measurements of these properties that often show large fluctuations in their pressure dependence (Poe et al., 1997). The phenomenological model given here can also be extended to the other systems, including fully polymerized aluminosilicates, by considering Si/Al dependence.

The Adam-Gibbs theory has been previously applied to describe the temperature dependence of viscosity in glass-forming liquids (Adam and Gibbs, 1965; Richet, 1984). Here, the pressure dependence of viscosity can be obtained as given below (e.g., Bottinga and Richet, 1995):

$$\left(\frac{\partial \eta}{\partial P}\right)_T = -\frac{A_{AG}}{TS_{config}} \exp\left(B_{AG} / TS_{config}\right) \times \left[\frac{B_{AG}}{S_{config}}\left(\frac{\partial S_{config}}{\partial P}\right)_T + \left(\frac{\partial B_{AG}}{\partial P}\right)_T\right], \quad (8)$$

where A_{AG} is a constant and the B_{AG} is related to the activation energy barrier for the cooperative rearrangement, and thus, we assume the pressure dependence of B_{AG} for Eqn. 8. Determining the configurational entropy from the structure of silicate melts can be rather ambiguous; entropy of mixing among structural units near the glass transition temperature has typically been used to model it (Neuville and Richet, 1991; Toplis et al., 1997; Lee and Stebbins, 1999). The NBO-fraction-dependent sign of $(\partial S_{config}/\partial P)_T$ was inferred from the Maxwell relations $[(\partial S/\partial P)_T = -(\partial V/\partial T)_P]$ and from the contribution for NBO-BO mixing entropy near T_g, which determines the pressure dependence of viscosity without considering $(\partial B_{AG}/\partial P)_T$ (Bottinga and Richet, 1995). Their approach could qualitatively explain the change in the sign of $(\partial \eta/\partial P)_T$ with NBO fraction (if $X_{NBO} < 0.5$, $(\partial \eta/\partial P)_T < 0$, and vice versa) below P_c (Bottinga and Richet, 1995). The model prediction (Eqns. 3, 4, and 5) is consistent with the result based on Adam-Gibbs theory when $\partial E_{NBO}/\partial P = -\partial E_{BO}/\partial P$ in Eqn. 5. Furthermore, our semiquantitative approach can explain the variation of diffusivity and viscosity above P_c by estimating the pressure dependence of the NBO fraction that can be experimentally obtained.

It is worthwhile mentioning that the effect of temperature on the molecular structures of silicate glasses and melts at ambient pressure has been studied extensively. These results showed changes of coordination environments of the framework cations in binary silicate and aluminosilicate glasses (e.g., Stebbins, 1991; Poe et al., 1992), strongly implying probable changes in local oxygen environments.

We have shown that the detailed structural information, particularly the connectivity among network polyhedra ($^{[4,5,6]}$Si or $^{[4,5,6]}$Al) as a function of pressure, can be directly estimated, allowing the evaluation of the degree of polymerization in silicate glasses and melts at high pressure. The model presented here can be used to account for the anomalous pressure dependence of silicate melt properties with composition and demonstrates that the fraction of NBO, as well as its pressure dependence, are critical in determining these properties. Together with previous studies of calculating the configurational thermodynamic properties from the atomic scale disorder (Lee and Stebbins, 2002), the results here provide another strong link between the atomic structures of melts and their macroscopic transport properties.

Acknowledgment—This research is supported by a Carnegie Postdoctoral Fellowship to L.S.K. We thank Drs. K. Mibe and G. Gudfinnsson for help with the multi-anvil experiments at the Geophysical Laboratory and Professor P. Grandinetti for RMN software for 2D NMR data processing. We also thank three anonymous reviewers for critical comments and constructive suggestions. Especially, insightful comments on the modeling by one of the reviewers greatly improved the clarity of the modeling part of the manuscript. We gratefully acknowledge the support of the W.M. Keck Foundation and the NSF for the NMR facility at the Geophysical Laboratory.

Associate editor: C. Romano

REFERENCES

Adam G. and Gibbs J. H. (1965) On the temperature dependence of cooperative relaxation properties in glass-forming liquids. *J. Chem. Phys.* **43,** 139–146.

Angell C. A. (1995) Formation of glasses from liquids and biopolymers. *Science* **267,** 1924.

Angell C. A., Cheeseman P. A., and Tamaddon S. (1982) Pressure enhancement of ion mobilities in liquid silicates from computer simulations studies to 800 kbar. *Science* **218,** 885–887.

Behrens H. and Schulze F. (2003) Pressure dependence of melt viscosity in the system $NaAlSi_3O_8$-$CaMgSi_2O_6$. *Am. Min.* **88,** 1351–1363.

Baltisberger J. H., Xu Z., Stebbins J. F., Wang S., and Pines A. (1996) Triple-quantum two-dimensional ^{27}Al magic-angle spinning nuclear magnetic resonance spectroscopic study of aluminosilicate and aluminate crystals and glasses. *J. Am. Chem. Soc.* **118,** 7209–7214.

Bertka C. M. and Fei Y. (1997) Mineralogy of the Martian interior up to core-mantle boundary pressures. *J. Geophys. Res.* **102,** 5251–5264.

Bottinga Y. and Richet P. (1995) Silicate melts: The "anomalous" pressure dependence of the viscosity. *Geochim. Cosmochim. Acta* **59,** 2725–2731.

Brearley M., Dickinson J. E., and Scarge C. M. (1986) Pressure dependence of melt viscosities on the join diopside-albite. *Geochim. Cosmochim. Acta* **50,** 2563–2570.

Brown G. E., Gibbs G. V., and Ribbe P. H. (1969) The nature and variation in length of the Si-O and Al-O bond in framwork silicates. *Am. Min.* **54,** 1044–1061.

Devine R. A. B. and Arndt J. (1987) Si-O bond-length modification in pressure-densified amorphous SiO_2. *Phys. Rev. B.* **35,** 9376–9379.

Diefenbacher J., McMillan P. F., and Wolf G. H. (1998) Molecular dynamics simulations of $Na_2Si_4O_9$ liquid at high pressure. *J. Phys. Chem. B.* **102,** 3003–3008.

Dirken P. J., Kohn S. C., Smith M. E., and Vaneck E. R. H. (1997) Complete resolution of Si-O-Si and Si-O-Al fragments in an aluminosilicate glass by O-17 multiple-quantum magic-angle-spinning NMR-spectroscopy. *Chem. Phys. Lett.* **266,** 568–574.

Dunn T. (1983) Oxygen chemical diffusion in three basaltic liquids at elevated temperature and pressure. *Geochim. Cosmochim. Acta* **47,** 1923–1930.

Frydman I. and Harwood J. S. (1995) Isotropic spectra of half-integer quadrupolar spins from bidimensional magic-angle-spinning NMR. *J. Am. Chem. Soc.* **117,** 5367–5368.

Giordano D. and Dingwell D. B. (2003) Non-Arrhenian multicomponent melt viscosity: a model. *Earth. Planet. Sci. Lett.* **208,** 337–349.

Hemley R. J., Mao H. K., Bell P. M., and Mysen B. O. (1986) Raman spectroscopy of SiO2 glass at high pressure. *Phys. Rev. Lett.* **57,** 747–750.

Kushiro I. (1976) Changes in viscosity and structure of melt of $NaAlSi_2O_6$ composition at high pressures. *J. Geophy. Res.* **81,** 6347–6350.

Kushiro I. (1983) Effect of pressure on the diffusivity of network-forming cations in melts of jadeite composition. *Geochim. Cosmochim. Acta* **47,** 1415–1422.

Kushiro I. and Mysen B. O. (2002) A possible effect of melt structure on the Mg-Fe^{2+} partitioning between olivine and melt. *Geochim. Cosmochim. Acta* **66,** 2267–2272.

Lee S. K. and Stebbins J. F. (1999) The degree of aluminum avoidance in aluminosilicate glasses. *Am. Mineral.* **84,** 937–945.

Lee S. K. and Stebbins J. F. (2000a) Al-O-Al and Si-O-Si sites in framework aluminosilicate glasses with Si/Al=1: quantification of framework disorder. *J. Non-Cryst. Solids.* **270,** 260–264.

Lee S. K. and Stebbins J. F. (2000b) The structure of aluminosilicate glasses: High-resolution ^{17}O and ^{27}Al MAS and 3QMAS NMR study. *J. Phys. Chem. B.* **104,** 4091–4100.

Lee S. K. and Stebbins J. F. (2002) The extent of inter-mixing among framework units in silicate glasses and melts. *Geochim. Cosmochim. Acta* **66,** 303–309.

Lee S. K. and Stebbins J. F. (2003) The distribution of sodium ions in aluminosilicate glasses: A high field Na-23 MAS and 3QMAS NMR study. *Geochim. Cosmochim. Acta* **67,** 1699–1709.

Lee S. K., Fei Y., Cody G. D., and Mysen B. O. (2003) Order and disorder of sodium silicate glasses and melts at 10 GPa. *Geophys. Res. Letts.* **30,** 1845.

Lee S. K. (2004) Structure of oxide glasses and melts at high pressure: Quantum chemical calculations and solid state NMR. *J. Phys. Chem. B.* **108,** 5889–5900.

Mazurin O. V. (1983) *Handbook of Glass Data: Silica Glass and Binary Silicate Glasses.* Elsevier Science.

Mysen B. O. (1988) *Structure and Properties of Silicate Melts.* Elsevier.

Mysen B. O., Virgo D., and Seifert F. A. (1982) The structure of silicate melts: implications for chemical and physical properties of natural magma. *Rev. Geophys. Space Phys.* **20,** 353–383.

Neuville D. R. and Richet P. (1991) Viscosity and mixing in molten (Ca, Mg) pyroxenes and garnet. *Geochim. Cosmochim. Acta* **55,** 1011–1019.

Poe B. T., McMillan P. F., Angell C. A., and Sato R. K. (1992) Al and Si coordination in SiO_2–Al_2O_3 glasses and liquids: A study by NMR and IR spectroscopy and MD simulations. *Chem. Geol.* **96,** 333–349.

Poe B. T., McMillan P. F., Rubie D. C., Chakraborty S., Yarger J. L., and Diefenbacher J. (1997) Silicon and oxygen self-diffusivities in silicate liquids measured to 15 Gigapascals and 2800 Kelvin. *Science* **276,** 1245–1248.

Poe B. T., Romano C., Zotov N., Civin G., and Marecelli A. (2001) Compression mechanisms is aluminosilicate melts: Rman and XANES spectroscopy of glasses quenched from pressures up to 10 GPa. *Chem. Geol.* **174,** 21–31.

Rao K. J., Kumar S., and Bhat M. H. (2001) A chemical approach to understand fragilities of glass-forming liquids. *J. Phys. Chem. B.* **105,** 9023–9027.

Reid J. E., Poe B. T., Rubie D. C., Zotov N., and Wiedenbeck M. (2001) The self-diffusion of silicon and oxygen in diopside ($CaMgSi_2O_6$) liquid up to 15 GPa. *Chem. Geol.* **174,** 77–86.

Richet P. (1984) Viscosity and configurational entropy of silicate melts. *Geochim. Cosmochim. Acta* **48,** 471–483.

Rosenhauer M., Scarfe C. M., and Virgo D. (1979) Pressure dependence of the glass transition in glasses of diopside, albite and sodium trisilicate compostion. *Carnegie. Inst. Washington Year Book* **78,** 556–559.

Scarfe C. M., Mysen B. O., and Virgo D. (1986) Pressure dependence of the viscosity of silicate melts. In *Magamatic Processes: Physicochemical Princeples* (ed. B. O. Mysen), pp. 59–68, The Geochemical Society.

Stebbins J. F. (1991) Experimental confirmation of five-coordinated silicon in a silicate glass at 1 atmosphere pressure. *Nature* **351,** 638–639.

Shimizu N. and Kushiro I. (1984) Diffusivity of oxygen in jadeite and diopside melts at high pressures. *Geochim. Cosmochim. Acta* **48,** 1295–1303.

Tinker D. and Lesher C. E. (2001) Self diffusion of Si and O in dacitic liquid at high pressures. *Am. Min.* **86,** 1–13.

Tinker D., Lesher C. E., and Hutcheon I. D. (2003) Self-diffusion of Si and O in diopside-anorthite melt at high pressures. *Geochim. Cosmochim. Acta* **67,** 133–142.

Toplis M. J., Dingwell D. B., Hess K. U., and Lenci T. (1997) Viscosity, fragility, and configurational entropy of melts along the join SiO_2-$NaAlSiO_4$. *Am. Mineral.* **82,** 979–990.

Waff H. S. (1975) Pressure-induced coordination changes in magmatic liquids. *Geophy. Res. Lett.* **2,** 193–196.

Wolf G. H. and McMillan P. F. (1995) Pressure effects on silicate melt structure and properties. In *Structure, Dynamics, and Properties of Silicate Melts*, Vol. 32 (ed. J. F. Stebbins et al.), pp. 505–562, Mineralogical Society of America.

Xu Z., Maekawa H., Oglesby J. V., and Stebbins J. F. (1998) Oxygen speciation in hydrous silicate glasses-An oxygen-17 NMR study. *J. Am. Chem. Soc.* **120,** 9894–9901.

Xue X., Stebbins J. F., Kanzaki M., and Tronnes R. G. (1989) Silicon coordination and speciation changes in a silicate liquid at high pressures. *Science* **245,** 962–964.

Xue X., Stebbins J. F., Kanzaki M., McMillan P. F., and Poe B. (1991) Pressure-induced silicon coordination and tetrahedral structural changes in alkali silicate melts up to 12 GPa: NMR, Raman, and infrared spectroscopy. *Am. Mineral.* **76,** 8–26.

Xue X., Stebbins J. F., and Kanzaki M. (1994) Correlations between O-17 NMR parameters and local structure around oxygen in high-pressure silicates and the structure of silicate melts at high pressure. *Am. Mineral.* **79,** 31–42.

Yarger J. L., Smith K. H., Nieman R. A., Diefenbacher J., Wolf G. H., Poe B. T., and McMillan P. F. (1995) Al coordination changes in high-pressure aluminosilicate liquids. *Science* **270,** 1964–1967.